2016

Coercivity and nanostructure of melt-spun Ti-Fe-Co-B-based alloys

Wenliang Zhang
University of Nebraska, Lincoln, wzhang15@unl.edu

Ralph A. Skomski
University of Nebraska-Lincoln, rskomski2@unl.edu

Arti Kashyap
University of Nebraska - Lincoln, akashyap@lnmiit.ac.in

Shah R. Valloppilly
University of Nebraska-Lincoln, svalloppilly2@unl.edu

Xingzhong Li
University of Nebraska-Lincoln, xli2@unl.edu

See next page for additional authors

Coercivity and nanostructure of melt-spun Ti-Fe-Co-B-based alloys

W. Y. Zhang,[1,2] R. Skomski,[1,2] A. Kashyap,[3] S. Valloppilly,[1] X. Z. Li,[1] J. E. Shield,[1,4] and D. J. Sellmyer[1,2]
[1]*Nebraska Center for Materials and Nanoscience, University of Nebraska, Lincoln, NE 68588 USA*
[2]*Department of Physics and Astronomy, University of Nebraska, Lincoln, NE 68588 USA*
[3]*School of Basic Sciences, Indian Institute of Technology, Mandi, Himachal Pradesh, India*
[4]*Department of Mechanical and Materials Engineering, University of Nebraska, Lincoln, NE 68588 USA*

(Presented 13 January 2016; received 2 November 2015; accepted 17 November 2015; published online 18 February 2016)

Nanocrystalline Ti-Fe-Co-B-based alloys, prepared by melt spinning and subsequent annealing, have been characterized structurally and magnetically. X-ray diffraction and thermomagnetic measurements show that the ribbons consist of tetragonal $Ti_3(Fe,Co)_5B_2$, FeCo-rich bcc, and NiAl-rich $L2_1$ phases; $Ti_3(Fe,Co)_5B_2$, is a new substitutional alloy series whose end members $Ti_3Co_5B_2$ and $Ti_3Fe_5B_2$ have never been investigated magnetically and may not even exist, respectively. Two compositions are considered, namely $Ti_{11+x}Fe_{37.5-0.5x}Co_{37.5-0.5x}B_{14}$ ($x = 0, 4$) and alnico-like $Ti_{11}Fe_{26}Co_{26}Ni_{10}Al_{11}Cu_2B_{14}$, the latter also containing an $L2_1$-type alloy. The volume fraction of the $Ti_3(Fe,Co)_5B_2$ phase increases with x, which leads to a coercivity increase from 221 Oe for $x = 0$ to 452 Oe for $x = 4$. Since the grains are nearly equiaxed, there is little or no shape anisotropy, and the coercivity is largely due to the magnetocrystalline anisotropy of the tetragonal $Ti_3(Fe,Co)_5B_2$ phase. The alloy containing Ni, Al, and Cu exhibits a magnetization of 10.6 kG and a remanence ratio of 0.59. Our results indicate that magnetocrystalline anisotropy can be introduced in alnico-like magnets, adding to shape anisotropy that may be induced by field annealing. [http://dx.doi.org/10.1063/1.4942552]

I. INTRODUCTION

Alnico magnets have recently attracted renewed attention due to rare-earth-supply concerns.[1–3] The magnets, which typically contain Fe, Co, Ni, Al, and various additives, have very good overall permanent-magnet properties but suffer from modest coercivities, which are limited to the shape-anisotropy contribution.[4–6] Several non-traditional ways to improve alnico magnets have been proposed. Embedded Co nanowires, with a columnar nanostructure similar to anisotropic alnicos, have been considered.[7] In $Fe_{30}Co_{70}$ nanowires, a naturally formed hard-magnetic oxide layer with a thickness of 3-4 nm, exchange coupled to a FeCo phase of dimension 40 nm, yields a 20% coercivity increase compared to shape-only anisotropy.[8] It is well-known that carbon doping yields a martensitic distortion of bcc Fe-Co.[9–11] Recently, it has been found that Mo doping induced the formation of the tetragonal structure for FeCo alloys, resulting in a magnetocrystalline anisotropy constant of 3.6 Mergs/cm^3 and a coercivity of 1.2 kOe for the Fe_8CoMo alloy.[12] The challenge is to realize such changes in an alnico-like microstructure.

The aim of this work is to create magnetocrystalline anisotropy by adding Ti and B to the melt-spun alloy. As we will show below, this leads the formation of a new tetragonal $Ti_3(Co,Fe)_5B_2$ alloy, which is a solid-solution derivative of $Ti_3Co_5B_2$ (space group P4/mbm). Figure 1 shows the schematic of the crystal structure of $Ti_3Co_5B_2$. There exist a variety of ternary, quaternary, and quinary ($A_2MT_{5-x}T'_xB_2$) derivatives of $Ti_3Co_5B_2$,[13–16] but this system has not been considered yet in

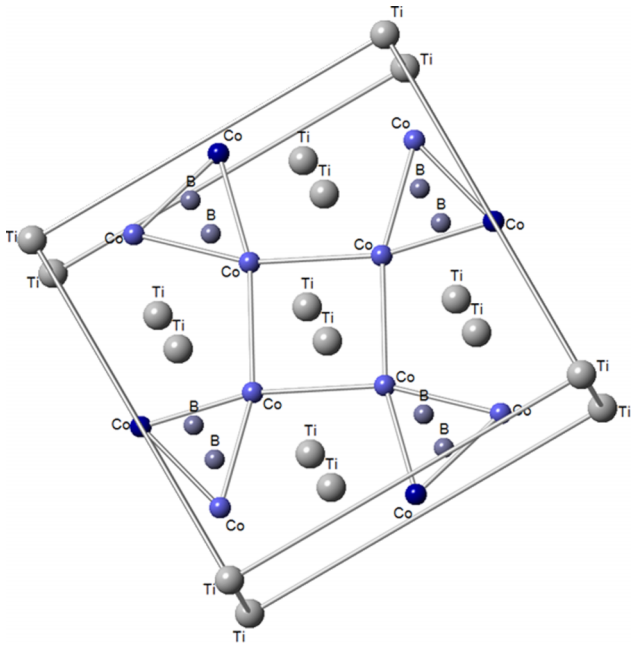

FIG. 1. Schematic of crystal structure of $Ti_3Co_5B_2$.

the context of alnico magnetism. In fact, even for archetypical $Ti_3Co_5B_2$, the magnetic properties are largely unknown, since the phase is difficult to prepare, and the isostructural $Ti_3Fe_5B_2$ phase may not exist at all.

II. EXPERIMENTAL METHOD

Ingots of $Ti_{11}Fe_{37.5}Co_{37.5}B_{14}$ (Sample I), $Ti_{15}Fe_{35.5}Co_{35.5}B_{14}$ (Sample II), and $Ti_{11}Fe_{26}Co_{26}Ni_{10}Al_{11}Cu_2B_{14}$ (Sample III) were arc melted from high-purity elements and CoB prealloy in an argon atmosphere. The ribbons were made by ejecting molten alloys in a quartz tube onto the surface of a copper wheel with a speed of 55 m/s. The melt-spun ribbons are amorphous. Typical ribbons are 2 mm wide and 50 μm thick. They were annealed in a tubular furnace, pumped to a base pressure of about 10^{-7} Torr at 650-750 °C for 10 min. The phase components were examined by Rigaku D/Max-B X-ray diffraction (XRD) with Co K_α radiation. The Rietveld analysis of the x-ray diffraction patterns was done using TOPAS software. The scanning transmission-electron microscopy (STEM) and element mapping were done with an FEI Tecnai Osiris transmission-electron microscope (TEM). The hysteresis loops and thermomagnetic curves were measured with a Quantum Design physical property measurement system (PPMS) and a vibration sample magnetometer at fields up to 70 kOe. The field is applied parallel to the long direction of the ribbons.

III. RESULTS AND DISCUSSION

Figure 2 shows XRD patterns of the three samples. Ribbons I and II consist of tetragonal $Ti_3(Fe,Co)_5B_2$ and Fe-Co-rich bcc phases, whereas the ribbons of Sample III contain the tetragonal 3:5:2, bcc, and NiAl-rich $L2_1$ phases. Quaternary derivatives of $Ti_3Co_5B_2$ tend to be partially ordered, of the type $A_3T_{5-x}T'_xB_2$. Depending on the occupancies of the 2c or 8j sites, there are well-defined $Ti_3Co_4FeB_2$ and $Ti_3CoFe_4B_2$ phases, but the present alloy is probably a solid solution of the composition $Ti_3(Fe_{2.5}Co_{2.5})_5B_2$.

The relative intensity of the diffraction peaks from the tetragonal $Ti_3(Fe,Co)_5B_2$ is highest for Sample II, indicating that these ribbons have the highest volume fraction of $Ti_3(Fe,Co)_5B_2$. Sample III has the lowest volume fraction of $Ti_3(Fe,Co)_5B_2$. According to the Scherrer equation, the

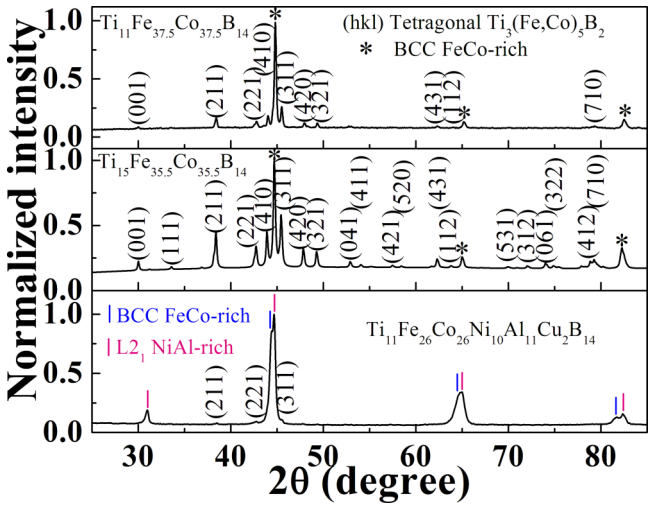

FIG. 2. XRD patterns of $Ti_{11}Fe_{37.5}Co_{37.5}B_{14}$ (I), $Ti_{15}Fe_{35.5}Co_{35.5}B_{14}$ (II), and $Ti_{11}Fe_{26}Co_{26}Ni_{10}Al_{11}Cu_2B_{14}$ (III).

respective mean grain sizes of the $Ti_3(Fe,Co)_5B_2$ and FeCo-rich phases are about 40 nm in Sample I, and about 30 nm in Sample II. This means that Ti addition somewhat refines the nanostructure of the Ti-Fe-Co-B ribbons.

In order to identify the magnetic phases in the ribbons, we have measured the magnetization as a function of temperature. Figure 3 indicates two ferromagnetic-to-paramagnetic phase transitions. The first one corresponds to the $Ti_3(Fe,Co)_5B_2$ phase. The second transition cannot be seen explicitly due to the temperature limitation and should come from the Fe-Co-rich phase. The Curie temperature of the $Ti_3(Fe,Co)_5B_2$ phase in the ribbons II is higher than that in the sample III, assuming that the signal comes from the 3:5:2 phase, not from the $L2_1$ phase. The Curie-temperature difference probably reflects different stoichiometries in the samples.

Element mapping is used to examine phase components of alloys, including nonmagnetic phases. Figure 4 shows the high-angle annular dark-field (HAADF) and element-mapping images of Sample I and III. The element mapping confirms our conclusions drawn from the XRD patterns. Sample I is composed of $Ti_3(Fe,Co)_5B_2$ and Fe-rich bcc phases. Sample III consists of the Ti-rich, Fe-rich and Ni-rich phases representing the tetragonal $Ti_3(Fe,Co)_5B_2$, FeCo-rich bcc, and NiAl-rich

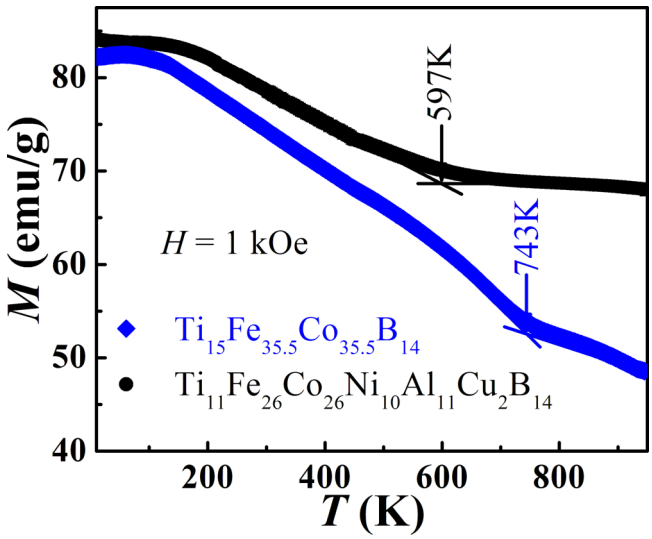

FIG. 3. $M(T)$ curves of $Ti_{15}Fe_{35.5}Co_{35.5}B_{14}$ (II), and $Ti_{11}Fe_{26}Co_{26}Ni_{10}Al_{11}Cu_2B_{14}$ (III).

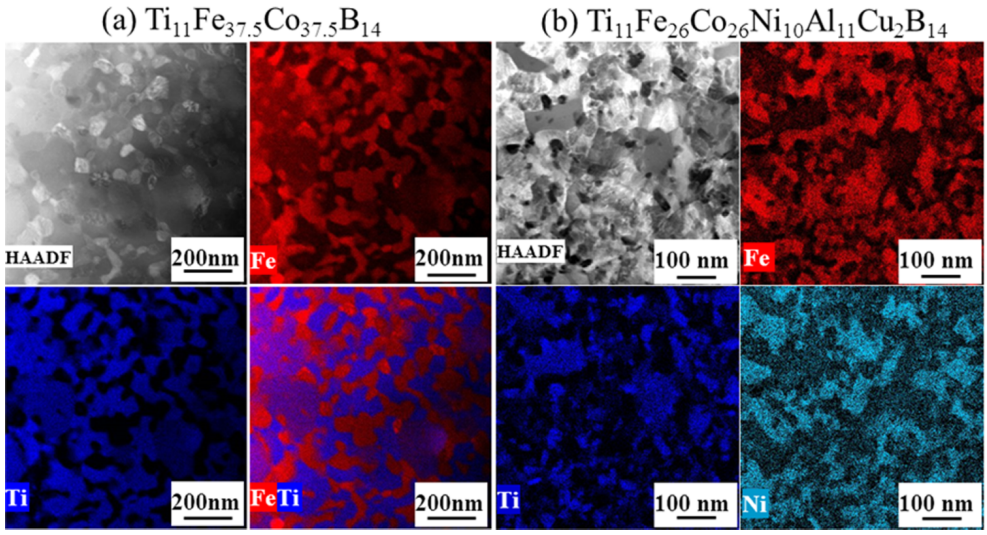

FIG. 4. HAADF and element mapping images of $Ti_{11}Fe_{37.5}Co_{37.5}B_{14}$ (I) and $Ti_{11}Fe_{26}Co_{26}Ni_{10}Al_{11}Cu_2B_{14}$ (III).

$L2_1$ structures. The contrast of the HAADF image is proportional to the atomic number. In Sample I, the average atomic number is smaller for $Ti_3(Fe,Co)_5B_2$ than for the FeCo-rich phase, so that the $Ti_3(Fe,Co)_5B_2$ phase looks darker than the FeCo-rich phase. In Sample III, the FeCo-rich phase has the largest average atomic number and $Ti_3(Fe,Co)_5B_2$ has the smallest one. Therefore, the FeCo-rich phase looks white, the $Ti_3(Fe,Co)_5B_2$ phase looks gray, and NiAl-rich phase looks light gray. The I and III ribbons crystallize or spinodally decompose to form nearly equiaxed nanograins. The grain sizes of the $Ti_3(Fe,Co)_5B_2$ and FeCo-rich phases are larger for sample I than for Sample III.

Figure 5 shows the room-temperature hysteresis loops of the samples I-III. The remanence ratio for all ribbons is larger than 0.5 due to the existence of intergrain exchange coupling. All ribbons exhibit some coercivity arising from the magnetocrystalline anisotropy of the tetragonal $Ti_3(Fe,Co)_5B_2$ phase. The coercivity of the ribbons increases with the concentration of the $Ti_3(Fe,Co)_5B_2$ phase, and the coercivity of Sample II is highest. Subject to the development of additional shape anisotropy by field annealing, the energy product of Sample III could be increased.

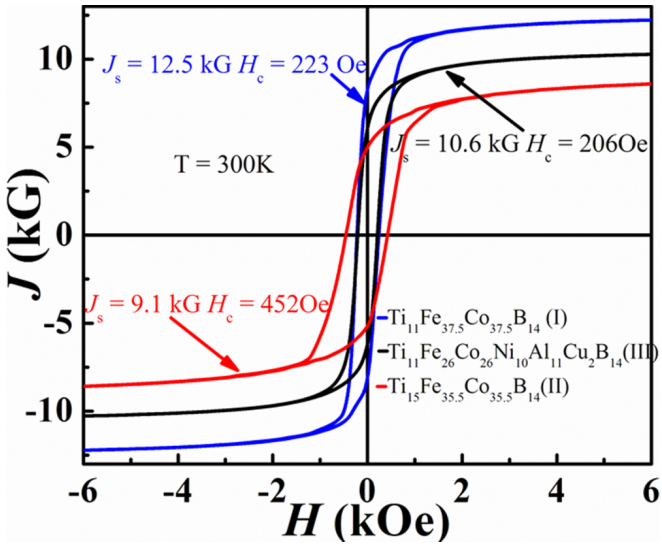

FIG. 5. Magnetization as a function of field for Sample (I), Sample (II), and Sample (III).

IV. CONCLUSIONS

We have investigated the structural and magnetic properties of Ti-containing alnico-like nanostructures. The nanocrystalline Ti-Fe-Co-B ribbons, fabricated by melt-spinning and annealing, contain $Ti_3(Fe,Co)_5B_2$, a new alloy crystallizing in the tetragonal $Ti_3Co_5B_2$ structure. The alloy exhibits a high Curie temperature and appreciable magnetocrystalline anisotropy, which leads to some coercivity and to a relatively high remanence ratio of about 0.6. The microstructure of the ribbons consists of equiaxed grains, so that there is almost no shape anisotropy, and the coercivity is therefore due to the tetragonal phase. The $Ti_3(Fe,Co)_5B_2$ phase can also be formed in alnico-like materials, which opens the prospect of combining shape and magnetocrystalline anisotropies.

ACKNOWLEDGEMENT

This work was supported by DoE/Ames Lab/DREaM project. The research was performed in part in the Nebraska Nanoscale Facility: National Nanotechnology Coordinated Infrastructure and the Nebraska Center for Materials and Nanoscience, which are supported by the National Science Foundation under Award ECCS: 1542182, and the Nebraska Research Initiative.

[1] M. J. Kramer, R. W. McCallum, I. A. Anderson, and S. Constantinides, JOM **64**, 752 (2012).
[2] C. Gaona-Tiburcio, F. Almeraya-Calderón, J. G. Chacon-Nava, J. A. Matutes-Aquino, and A. Martinez-Villafañe, J. Alloy Compd **369**, 78 (2004).
[3] R. W. McCallum, L. H. Lewis, R. Skomski, M. J. Kramer, and I. E. Anderson, Annual Review of Materials Research **44**, 451 (2014).
[4] D. A. Oliver and J.W. Shedden, Nature **142**, 209 (1938).
[5] C. Bronner, J. -P. Haberer, E. Planchard, and J. Sauze, Cobalt **46**, 15 (1970).
[6] Y. L. Sun, J. T. Zhao, Z. Liu, W. X. Xia, S. M. Zhu, D. Lee, and A. R. Yan, J. Magn. Magn. Mater. **379**, 58 (2015).
[7] K. Gandha, K. Elkins, N. Poudyal, X. B. Liu, and J. P. Liu, Sci. Rep. **4**, 5345 (2014).
[8] S. Liébana Viñas, R. Salikhov, C. Bran, E. M. Palmero, M. Vazquez, B. Arvan, X. Yao, P. Toson, J. Fidler, M. Spasova, U. Wiedwald, and M. Farle, Nanotechnology **26**, 415704 (2015).
[9] E. K. Delczeg-Czirjak, A. Edström, M. Werwiński, J. Rusz, N. V. Skorodumova, L. Vitos, and O. Eriksson, Phys. Rev. B **89**, 144403 (2014).
[10] R. Skomski, V. Sharma, B. Balamurugan, J. E. Shield, A. Kashyap, and D. J. Sellmyer, in *Proc. REPM'10*, edited by S. Kobe and P. McGuinness (Jozef Stefan Institute, Ljubljana, 2010), pp. 55–60.
[11] R. M. Bozorth, *Ferromagnetism* (van Nostrand, Princeton, New Jersey, 1951).
[12] A. G. Kusne, T. R. Gao, A. Mehta, L. Q. Ke, M. C. Nguyen, K. M. Ho, V. Antropov, C. Z. Wang, M. J. Kramer, C. Long, and I. Takeuchi, Sci. Rep. **4**, 6367 (2014).
[13] W. Jung, J. Schiffer, and Z. Anorg, Allg. Chem. **581**, 135 (1990).
[14] E. A. Nagelschmitz and W. Jung, Chem. Mater. **10**, 3189 (1998).
[15] E. A. Nagelschmitz, W. Jung, R. Feiten, P. Müller, H. Lueken, and Z. Anorg, Allg. Chem. **627**, 523 (2001).
[16] P. Villars and K. Cenzual, Pearson's Crystal Structure Database for Inorganic Compounds (on CD-ROM), Version 1.0, Materials Park, OH, USA, 2007/8.